Int. J. Nanoelectronics and Materials **9** (2016) 49-66

Biosynthesis of (ZnO–Aloe vera) Nanocomposites and Antibacterial/Antifungal Studies

A. Ayeshamariam[1,], M. Kashif[2], V. S. Vidhya[3], M. G. V. Sankaracharyulu[4], V. Swaminathan[5], M. Bououdina[6,7], M. Jayachandran[8]*

[1] *Department of Physics, Khadir Mohideen College, Adirampattinam 614 701, India*
[2] *Nano Biochip Research Group, Institute of Nano-Electronic Engineering (INEE), Universiti Malaysia Perlis (UniMAP), Kangar 01000, Perlis, Malaysia*
[3] *Department of Chemistry, Chendhuran College of Engineering and Technology, Pudukottai, 622 507, India*
[4] *Arignar Anna Government Arts & Science College, Karaikal, Karaikal District, 609605, India*
[5] *School of Material Science and Engineering, Nanyang Technological University, Singapore 639798, Singapore*
[6] *Nanotechnology Centre, University of Bahrain, PO Box 32038, Kingdom of Bahrain*
[7] *Department of Physics, College of Science, University of Bahrain, PO Box 32038, Kingdom of Bahrain*
[8] *Electro Chemical Material Science Division, (CSIR) Central Electro Chemical Research*

Received 28 May 2014; Revised 23 March 2015; Accepted 4 May 2015

Abstract

Development of disease treatment and preventive measures to avoid any dangerous outbreak of epidemic proportions are important. Modern methods of detection and treatment include tissue culture, nanotechnology, radiation, and laser technology. We report the synthesis of nanocrystalline materials by combustion method with the use of *Aloe vera* extract powder. Addition of ZnO changes the structural and optical properties of *A. vera*. The as-prepared nanocrystalline ZnO (ZnO + *A. vera*) powders were characterized using XRD, TEM, and SEM. Antibacterial and antifungal tests show that ZnO nanoparticles mixed with *A. vera* are effective in inhibiting bacterial growth.

Keywords: Morphology**,** Structural; Optical, Bacterial
PACS: 68.49.Df, 61.46.Df, 78.20.-e, 87.19.xb.

1. Introduction

Researchers have focused on development of efficient environmental friendly methods for synthesis of nanoparticles (NPs) on an anvil. Among these techniques, plants are the most promising candidates because of their ability to biosynthesize NPs in a large scale. The use of NPs shortens the synthesis time and results in a more effective treatment, and results in a more effective treatment, whereas the use of chemically formulated drugs

[*]) For Correspondence;E-mail: aismma786@gmail.com

is time consuming. Chemical formulation also causes serious side-effects because the chemicals that are absorbed by the body are rarely excreted, which ultimately damage the natural defense of the body.

ZnO presents high electron mobility, high thermal conductivity, good transparency, wide and direct bandgap of 3.37 eV, and high exciton binding energy; ZnO can also be grown easily in various nanostructure forms. These unique and excellent properties make ZnO suitable for various applications, such as in optoelectronics, transparent electronics, and lasing and sensing applications [1].

Moreover, ZnO preferentially exists in a stable hexagonal wurtzite structure at room temperature, in which each oxygen ion is surrounded by tetrahedral zinc ions alternatively stacked along the *c*-axis. Its crystallization properties are vital in crystal growth, defect generation, and etching. Investigation on the optical properties of ZnO has been conducted since 1960s [2]. ZnO has recently elicited attention among wide bandgap materials because of its direct wide bandgap (3.37 eV) with high exciton energy (60 meV) at room temperature [3].

Alternatively, semiconducting oxides, such as SnO_2 and In_2O_3, have become important. In particular, In_2O_3 as a transparent semiconductor with a direct wide-bandgap of approximately 3.6 eV and an indirect bandgap of approximately 2.5 eV [4], has been widely used in solar cells, organic light-emitting diodes, batteries, and transparent thin film infrared reflectors [5]. Both ZnO and In_2O_3 have been reported to react at high temperature (>1000 °C) to form a series of homologous compounds [6].

A new method reported by Maensiri et al. produces In_2O_3 NPs with particle size of 5 mm to 50 nm by using indium acetylacetonate and *Aloe vera* extract solution [7]. This simple process, which uses cheap precursors of *A. vera* extract, provides high-yield nanosized materials with well-defined crystalline structure and good optical properties. This method can also be adopted to prepare various nanocrystalline oxides. Renugadevi and Ashwini [8] reported the biological synthesis of NPs, in which the reducing agent can be any bio-source. Silver NPs were synthesized using *Azadirachta indica* leaf extract as a reducing agent by microwave irradiation method.

Aloe barbadensis Miller (*A. vera*) is a perennial plant of the Liliaceae or Aloeaceae family. *Aloe* has naturalized throughout the warm regions around the world. The genus *Aloe* contains over 400 different species, among which, *A. barbadensis* Miller (*A. vera*), *A. aborescens*, and *A. chinensis* are the most popular. *A. barbadensis* Miller is the most biologically active among these species [9]. In addition, *A. vera* gel contains vitamins A (beta-carotene), C, and E, which are known antioxidants. *A. vera* also has calcium, chromium, copper, selenium, magnesium, manganese, potassium, sodium, and zinc, which are essential for proper functioning of various enzyme systems in different metabolic pathways, and several of these elements also act as antioxidants. *A. vera* gel provides four plant steroids, namely, cholesterol, campesterol, β-sisosterol, and lupeol, which offer anti-inflammatory action. Lupeol also presents antiseptic and analgesic properties, providing 20 out of the 22 required amino acids in humans and 7 out of the 8 essential amino acids. This plant steroid also contains salicylic acid, which possesses anti-inflammatory and antibacterial properties. When lignin, an inert substance, is included in topical preparation, the penetrative effect of other ingredients into the skin is enhanced. Saponins, which are soapy substances, form approximately 3% of the gel and present cleansing and antiseptic properties [10]. Moreover, *A. vera* gel is a viscous, colorless, transparent, and odorless liquid with a slightly bitter taste. In general, identity tests are established in accordance with national requirements, usually for its polysaccharide composition, as shown in Fig. 1.

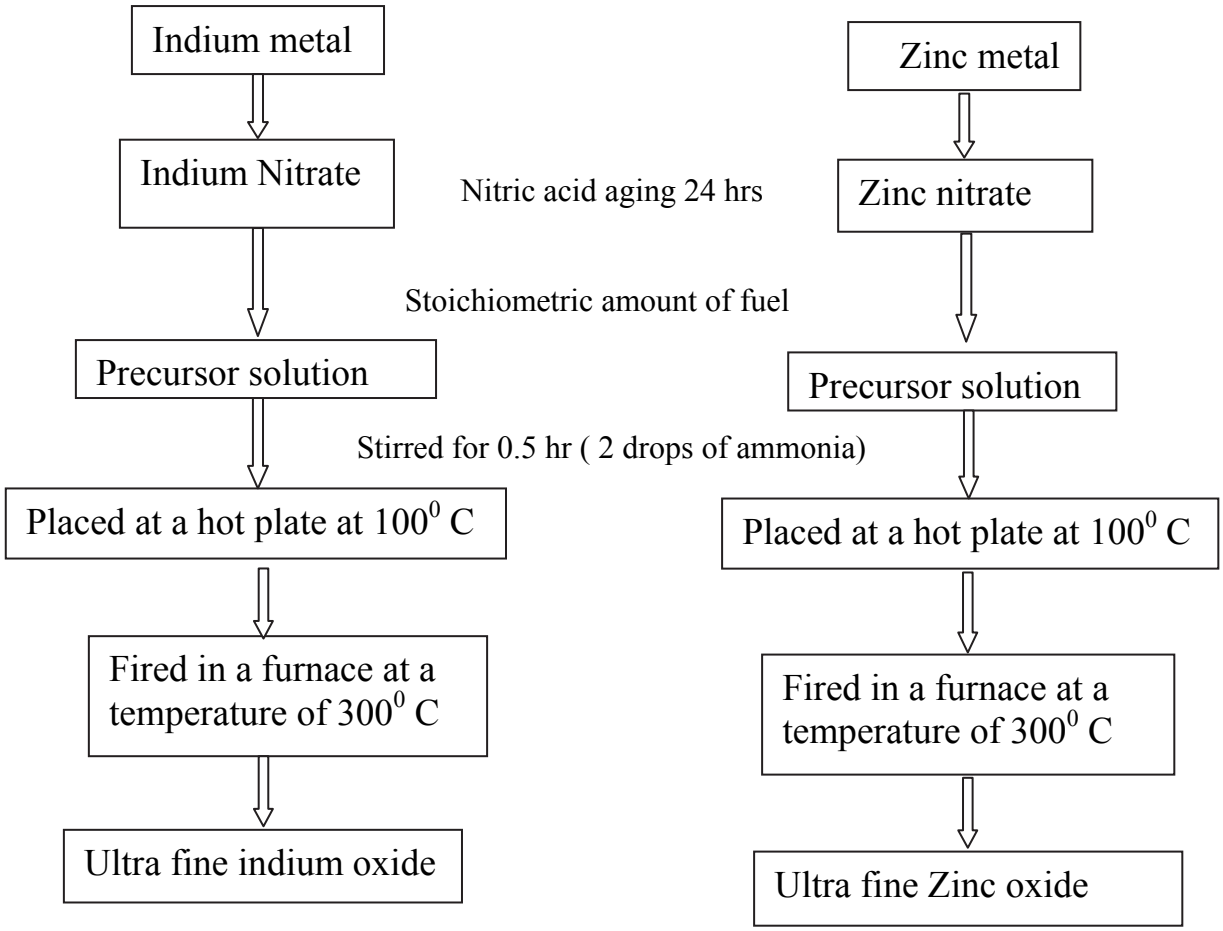

Fig. 1: Schematic preparation route of In_2O_3 and ZnO nanoparticles

Biological methods using plant extracts and microorganism have been proposed as alternative environmental friendly methods to synthesize metallic NPs because chemically formulated drugs cause side-effects.

In the current study, a novel synthesis for In_2O_3 and ZnO NPs, with particle sizes ranging from 10 nm to 30 nm using indium nitrate and zinc nitrate solutions, is reported. NPs are formed by combustion of dried precursors in a furnace at 300 °C for 3 min. This method utilizes *A. vera* extract from the solution as a solvent instead of organic solvents. Pure extract powders are prepared by using the method in a previous report [11]. This method is inexpensive, nontoxic, and uses environmentally safe precursors. This cost-efficient source of *A. vera* extract provides high-yield nanosized materials with good crystalline structure and good optical properties. The proposed method can also be used to prepare nanocrystalline oxides of other materials.

The antibacterial activities of synthesized NPs (ZnO and In_2O_3) have also been studied. The antibacterial activities of ZnO, In_2O_3, *A. vera* + ZnO, *A. vera* + In_2O_3, and ZnO + In_2O_3 + *A. vera* NPs have been assessed against the microorganisms *Staphylococcus aureus*, *Escherichia coli*, *Salmonella typhi*, *Pseudomonas aeruginosa*, and *Streptococcus pyogenes*, as well as antifungal microorganism *Aspergillus niger*, by disc diffusion method.

2. Experimental procedure

2.1 Samples Preparation

A solution (0.5 M) containing In $(NO_3)_3 \cdot 3H_2O$ and $Zn(NO_3)_2 \cdot 6H_2O$ was prepared in water. Afterwards, an ammonia solution was added drop-wise into the mixed precursor solution until its pH reached 6. The mixture was then diluted with water and magnetically stirred for 1 h. Urea was added as an oxygen-balancer to the mixture until a gel of indium oxide and zinc oxide was obtained. The mixture was stirred for another 1 h at ambient temperature. The pH of the solution was maintained in the range of 5 to 6. The solution was stirred again for 1 h to ensure complete precipitation. The solution was then placed on a hot plate at 100 ºC until its decomposition into a gel-like foam structure. The product was placed in a furnace and fired at 300 °C to obtain the dried nanopowder.

2.2 Characterization Techniques

X-ray diffraction (XRD) was performed using a Philips XRD with Cu-Kα radiation (λ = 0.15406 nm). The particle size and morphology of the calcined powders were characterized by transmission electron microscopy (TEM, Hitachi H8100 200 kV). Scanning electron microscopy (SEM) analysis was conducted using Hitachi S-4500 SEM machine. Optical absorption spectra were measured from 200 nm to 800 nm using a Shimadzu UV-3101PC UV–VIS–NIR spectrophotometer. Photoluminescence (PL) measurement was performed on a PL spectrometer Perkin–Elmer LS-55B using a xenon lamp as excitation source at room temperature (the samples were dispersed in dichloromethane) and with an excitation wavelength of 250 nm

2.3 Extraction of antimicrobial ingredients from A. vera leaves

The powder was obtained from the *A. vera* leaf extract solution in a freeze dryer by rapidly freezing the peel and then eliminating water by sublimation. The phosphatebuffered saline used in this study contained a final concentration of 137 mM of sodium chloride, 2.7 mM of potassium chloride, 4.3 mM of sodium phosphate (dibasic), and 1.4 mM of potassium phosphate (monobasic). Distilled water (DW) was used for extraction, which is economically desirable for large-scale industrial applications [9]. Exactly 50 g of the material was added to 500 ml of DW and was shaken at a speed of 250 rpm for 8 h at room temperature. The solution was then centrifuged at 3000 rpm for 50 min. The supernatant was filtered through No. 5A filter paper, and the filtered solution was again freeze-dried. A total of 1 g of the dried powder was dissolved in 1.5 ml of DW to form a saturated solution.

2.4 Preparation of Nanocomposites

To obtain *A. vera* leaf extract and oxide nanocomposite materials, 1 g of dried powders (ZnO and In_2O_3) were separately dissolved in 1.5 ml of DW. Equal ratios of these two solutions were thoroughly stirred and dried using a hot plate at 40 ^oC (natural temperature of *A. vera* leaf extract). A total of 1 g of In_2O_3 and 1 g of ZnO powder with the same ratio of *A. vera* dried powder were separately dissolved in two 1.5 ml portions of DW to obtain the nanocomposite dried powder.

2.5 Evaluation of antibacterial and antifungal activities

The supernatant was collected and stored in a refrigerator at 4 °C. Different concentrations of *A. vera* extracts were subjected to antimicrobial studies. Five bacterial cultures were maintained in nutrient agar medium at room temperature and sub-cultured into newly prepared nutrient agar slants every two weeks.

2.5.1 Well Diffusion Method

The antibacterial and antifungal activities of the plant extracts were tested using well diffusion method [12]. The prepared culture plates were inoculated with different strains of bacteria and fungi using streak plate method. Wells were made on the agar surface using a 5 mm cork borer. The extracts were poured into the well using a sterile syringe. The plates were incubated at 37± 2°C for 48 h for fungal activity and for 24 h for bacterial activity. The plates were observed for zone formation around the wells.

A. vera extracts, nanocomposite oxides ZnO and In_2O_3, *A. vera* + ZnO, *A. vera* + In_2O_3 and *A. vera* + ZnO + In_2O_3 were used throughout the study. The extracts were dissolved in sterile DW to form dilutions with 5, 10, and 25 µg of the extracts. Each concentration of the drug was tested against different bacterial pathogens for antibacterial activity using well diffusion assay [13]. One species each of Gram-positive bacteria and Gram-negative bacteria (*P. aeruginosa* MTCC-3542) were used for antibacterial assays.

The zone of inhibition was calculated by measuring the diameter of the inhibition zone around the well (in mm), including the well diameter. Readings were obtained in three different fixed directions in all three replicates, and the average values are provided in Table 2.

The methanolic and aqueous extracts of 100, 200, and 500 mg *A. vera* extract powder, *A. vera* extract with ZnO, *A. vera* extract with In_2O_3, and *A. vera* powder with ZnO and In_2O_3 were used for determination of antifungal activities.

(a) Bacterial Media (Muller–Hindon medium)

A total of 36 g of Muller–Hindon medium (Hi-medium) was mixed with DW and then sterilized in an autoclave at 15 liquid bowl pound (lbp) pressure for 15 min. The sterilized media were then poured onto Petri dishes. Pores were formed in the solidified plates by using a 5 mm diameter cork borer. Plates with wells were used for the antibacterial studies. Other solidified plates were pored using a 6 mm diameter cork borer.

(b) Fungal Media (Sabouraud agar medium)

A total of 10 g of peptone was mixed with DW, and 40 g of dextrose was mixed with the peptone infusion. Then, 20 g of agar was added as a solidifying agent. These constituents were mixed and autoclaved. The solidified plates were pored using a 5 mm diameter cork borer.

(c) Bacterial Strains

Bacterial and fungal pathogenic strains were obtained from the Microbial Type Culture Collection (MTCC), the Institute of Microbial Technology, Sector 39-4 Chandigarh, India. Bacterial strains included *S. aureus* (MTCC-737), *S. pyogenes* (MTCC-1923), *P. aeruginosa* (MTCC-3542), *E. coli* (1576), and *S. typhi* and were maintained at 4 ^{o}C on nutrient agar.

(d) Fungal Strains

Fungal strains were *A. niger* (MTCC-1344), *A. flavus* (MTCC-1973), *A. fumigatous* (MTCC-2132), *Rhizopusindicus*, and *Mucorindicus* (MTCC-918).

3. Results and discussion

3.1 Structural Characterization

The XRD pattern of ZnO powder confirms the presence of a high-quality hexagonal wurtzite crystalline structure (Fig. 2a), which is in agreement with JCPDS, Card No. 36-1451 [4], with lattice parameters a = 3.249 Å and c = 5.206 Å, and mean crystallite size of around 27 nm, as calculated using Sheerer's equation.

In_2O_3 crystallizes within the C-M_2O_3 (bixbyite) structure, which is in agreement with JCPDS Card No. 6-416) [4], with lattice *parameter a* = 10.117 Å and mean crystallite size of around 11 nm, as calculated using Sheerer's equation (Fig. 2). The observed reflections are assigned to the (222) and (400) planes, indicating a preferential growth of crystallites along the (222) plane. The effective surface area for ZnO and In_2O_3 decreases because of the incorporation of *A. vera*, thereby decreasing their optical activities. When *A. vera* is doped with ZnO, In_2O_3 optical properties show the lowest adsorption of extract, and their initial value of saturation is extremely low in comparison with that of other samples. For the present case, the observed large crystal sizes confirm that no dependency between the energy gap and the crystal size would be expected.

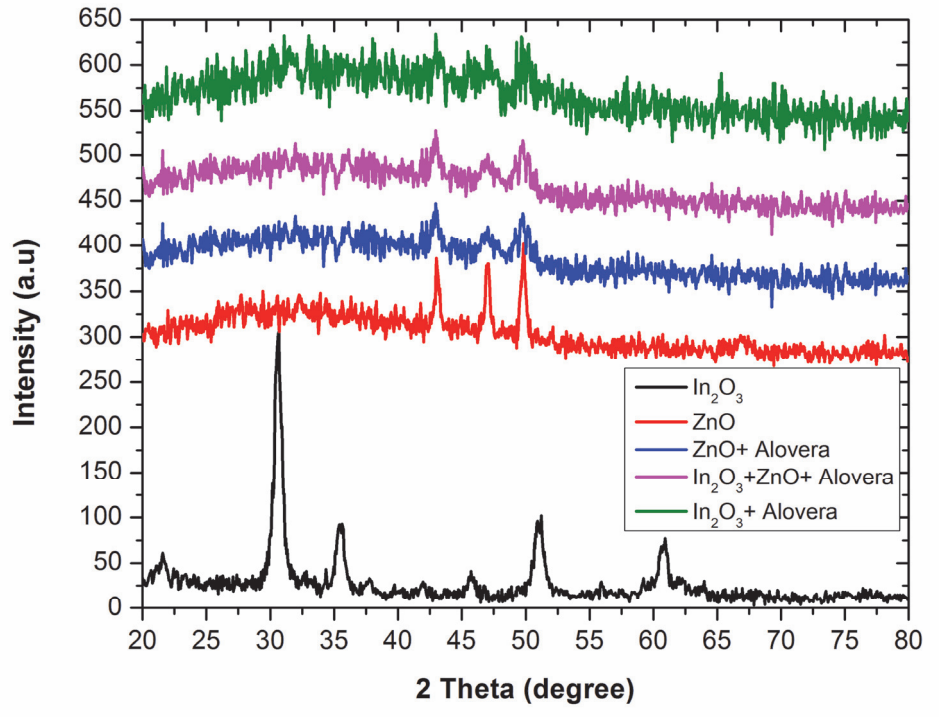

Fig. 2: XRD results of all the samples except *alovera* powder

A decrease in dispersion stability by the incorporation of *A. vera* would also result in less absorption of *A. vera* extract on the surface, and may be the reason for low degradation.

Therefore, higher *dopant* concentration results in less effective surface absorption of *A. vera*, which is necessary for reactions and lower degradation of *A. vera*.

Uniform particle size distribution is important for nanocrystalline systems. However, the addition of *A. vera* to oxide materials (In_2O_3 and ZnO) to form nanocomposites results in an increase in particle size. If segregation of additives occurs, then both In_2O_3 and ZnO particles are agglomerated with *A. vera* extract powder, thereby decreasing the crystallinity of the powder. Given that the XRD pattern of In_2O_3 + *A. vera* presents typical patterns of amorphous phases, calculating the full width at half maximum, which helps to estimate the crystallite size, is impossible. For ZnO + *A. vera*, only one peak is observed, with minimum relative intensity giving a mean crystallite size of 69 nm. For ZnO + In_2O_3 + *A. vera* composite, the estimated crystallite size is approximately 47 nm, and the XRD pattern shows a crystallized powder with no uniformity (Table 1).

If the crystallite size of pure ZnO and In_2O_3 becomes smaller, then the surface area remarkably increases hence, the surface properties are important and considered determinants of the properties of the as-prepared nanocomposites. Thus, diffusion and hygroscopicity of particles may occur when the nanomaterials are mixed with *A. vera* extract, resulting in a possible decrease in surface area, which consequently reduces surface energy

Table 1: XRD results of ZnO, *Alovera* + ZnO, In_2O_3, *Alovera* + In_2O_3, and *Alovera* + ZnO + In_2O_3

Sample	**Particle size (nm)**	**Strain=** $\beta \cos\theta / 4$	**Dislocation density** $\frac{1}{D^2}$ **lines/m^2**	**Lattice parameter**	**Volume (m^3)**
ZnO	27.33	0.0053	1.339 x 10^{15}	a = 3.248 c = 5.192 c/a = 1.598	$a^2{}_{C\ Sin\theta}$ = 47.104
Alovera + Zin oxide	69.02	0.01218	2.099 x 10^{14}	a = 3.112 c = 5.001 c/a = 1.607	$a^2{}_{C\ Sin\theta}$ = 41.94
Indium oxide	11.010	0.00329	0.8249 x 10^{16}	10.22	a^3 = 1067.09
Alovera Indium oxide + Zinc oxide	47.32	0.02145	4.527 x 10^{14}	a = 2.963 c = 5.023 c/a = 1.695	$a^2{}_{C\ Sin\theta}$ = 38.189

3.2 TEM Analysis

The high-resolution lattice images suggest that the nanopowders are crystalline. The distance between two lattice planes is similar in ZnO and In_2O_3 phases, which corresponds to the d-spacing of (001) crystal planes of wurtzite ZnO. The TEM images in Figs. 3a and 3b show ZnO + *A. vera* and In_2O_3 + *A. vera* composites. Significant changes are observed in particle morphology because of the addition of *A. vera* in the ZnO + In_2O_3 + *A. vera* composite (Fig. 3a). The TEM image of ZnO + In_2O_3 + *A. vera* nanocomposite confirms the general morphologies seen in SEM observation (Section 3.3). Individual belt-like nanostructures frequently exhibit a doped-crystal nature with obvious contours. The ends of these nanobelts exhibit peculiar morphologies, such as irregular-triangle heads.

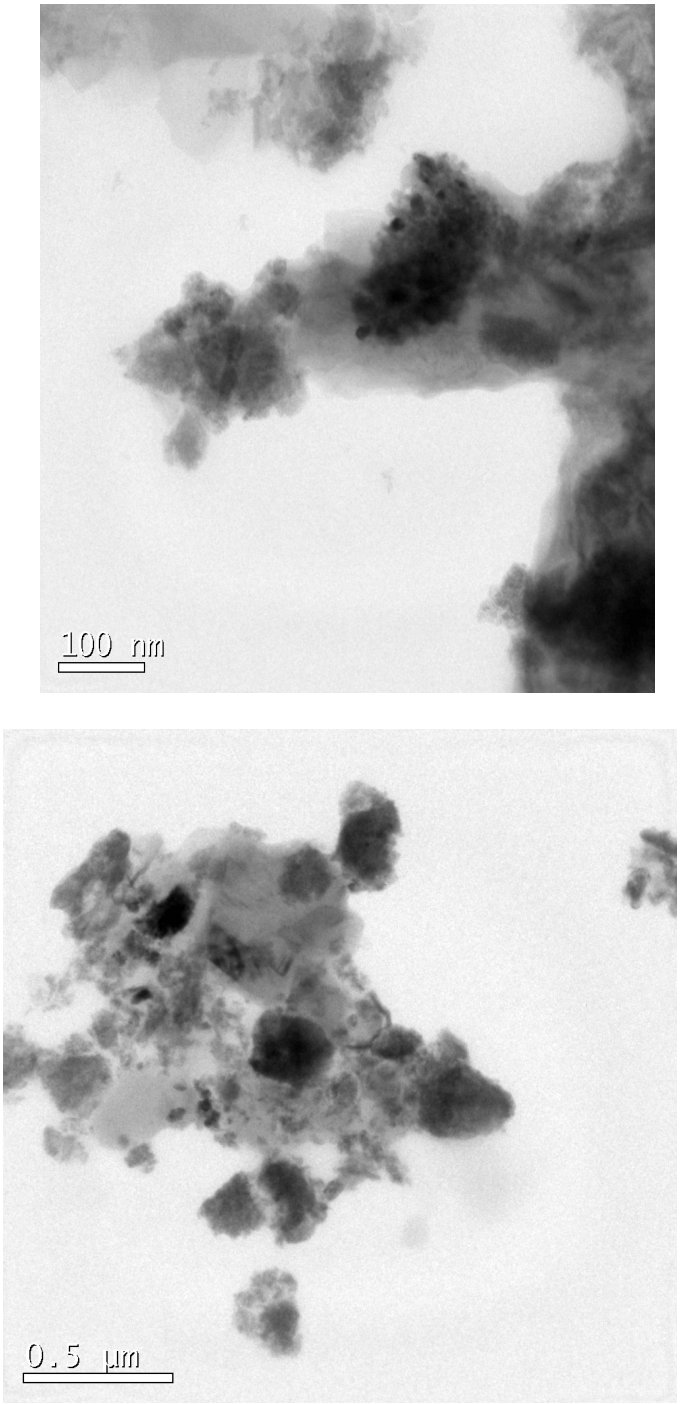

Fig. 3: (a). TEM image of (ZnO + Alovera), Fig. 3: (b). TEM image of (In_2O_3 + Alovera)

Such peculiar structures are further analyzed in detail using analytical TEM. The bright-field TEM images of a ZnO + In_2O_3 + *A. vera* with an irregulartriangle head are shown in Fig. 3c. The diagram for the lattice structure of diffraction pattern is also shown in Fig. 3d. The diameter of the belt is approximately 60 nm, and its length reaches up to 50 mm (shown in this figure). The bright–dark stripes in the body of the nanostructures (indicated by the arrows) are mostly ZnO (110) and (001) planes. For In_2O_3, a multiple crystalline nature of the nanocomposites is observed.

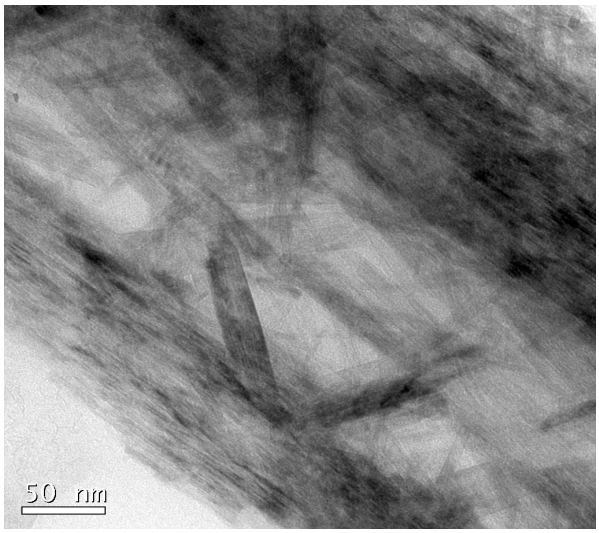

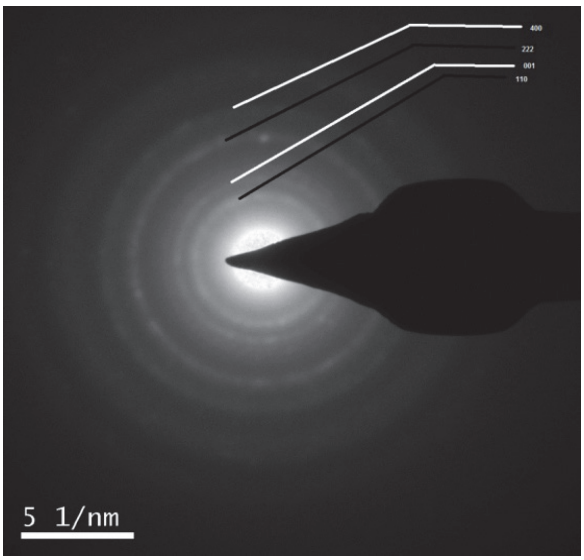

Fig. 3: (c) TEM image of (ZnO + In_2O_3 + *Alovera*), Fig. 3: (d). SAED pattern of (ZnO + In_2O_3 + *Alovera*)

A significant change is observed in the morphology of ZnO + In_2O_3+ *A. vera* nanocomposite, which possesses more oxygen vacancies with appropriate ratios reflected in the UV–Vis spectroscopy (Section 3.3). ZnO and In_2O_3 combined with *A. vera* powder show microstructures (TEM and SEM) that are prone to quick agglomeration (80 nm clusters). No further annealing is applied to avoid such agglomeration. The TEM image of In_2O_3 + *A. vera* and ZnO + *A. vera* NPs exhibits large sizes and shapes ranging from 80 nm to 100 nm. For ZnO + In_2O_3 + *A. vera* particles, the size decreases up to approximately 50 nm. Therefore, ZnO + In_2O_3 + *A. vera* nanocomposite produces extremely small particles with a predominant ZnO (110) reflection.

3.3 SEM Analysis

The SEM images of In_2O_3, ZnO, ZnO + *A. vera*, In_2O_3 + *A. vera*, and ZnO + In_2O_3 + *A. vera* nanopowders are interconnected, but the third nanocomposite presents a three-dimensional structure (Fig. 4), with good mechanical strength, as observed in its TEM image. The microstructural changes during the process incorporating *A. vera* lead to a

decrease in pore size and diameter, resulting in particle agglomeration. These microstructural changes are accompanied by associated internal stresses in the membrane of nanocomposites. Adding *A. vera* to ZnO and In_2O_3 can lead to local shifts in the interconnected grains, thereby reducing internal stresses. This observation results in a decrease in bandgap of the nanocomposite (see Section 3.4). The SEM morphology of the oxide product strongly depends on the precursor system, and its composites (ZnO + In_2O_3) exhibit good incorporation of *A. vera* extracts, in which a well-defined and easily accessible crystal surface is observed. However, the SEM images reveal a surface layer with different crystallinity that may explain the high content of ZnO + In_2O_3 at the *A.vera* surface. Given that no other crystalline structure different from ZnO was found on the XRD data, *A.vera* must be amorphous and possess a high In content, which is probably In_2O_3. This effect is important because the lesser formation may be related to the slow growing rate of these nanocomposites.

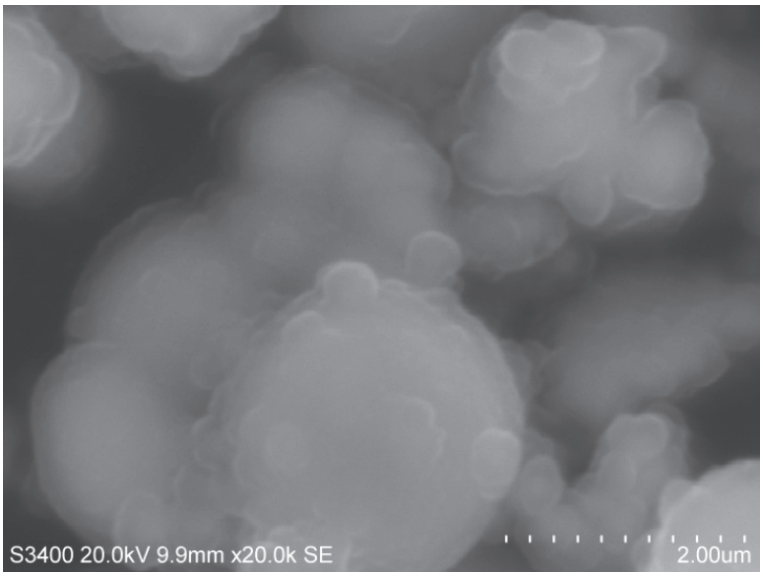

Fig. 4: SEM photograph of (ZnO + In_2O_3 + *Alovera*)

3.4 Optical Studies

Semiconducting NPs exhibit a change in electronic properties relative to their bulk counterpart. As the size of the particles decreases, the bandgap increases. Likewise, as *A. vera* extracts are mixed with ZnO, In_2O_3, and ZnO + In_2O_3, bulk bandgap energies shift to the red region. In other words, particle size increases, resulting in the decrease of bandgap value. However, the results of pure ZnO and In_2O_3 are enhanced in the third nanocomposite (unclear).

ZnO, In_2O_3, ZnO + *A. vera*, and In_2O_3 + *A. vera* composites rapidly turn dark green, whereas ZnO + In_2O_3 + *A. vera* powder turns black. The absorption band in the NIR region is shown in Fig. 5a.

Optical absorption and emission spectra of ZnO + *A. vera*, In_2O_3 + *A. vera*, and ZnO + In_2O_3 + *A. vera* show that the related absorption or emission peak shifts toward the red region as particle size increases (Fig. 5a). However, even the most highly colored products present low optical absorption in the visible region of the spectrum. Thus, in this case, the nanocomposites can also be considered transparent conductors.

UV–Vis spectroscopy showed that, although ZnO and In_2O_3 exhibit UV emissions that can be attributed to excitonic transitions, UV emissions of ZnO + *A. vera*, In_2O_3 + *A.*

vera, and ZnO + In_2O_3 + *A. vera* could also be due to deep-level defects, which are associated with oxygen deficit (vacancies) and interstitial Zn ions (structural defect). Therefore, the slow growth rate (lower potential deposition) would result in a stronger effect in ZnO compound. An appropriate choice of experimental parameters is crucial to suppress or enhance the defect-related emission of ZnO. This finding indicates that surface states are extremely important to the optical properties of NPs. The peaks at 486 and 520 nm may be due to Zn vacancy-related defects [14].

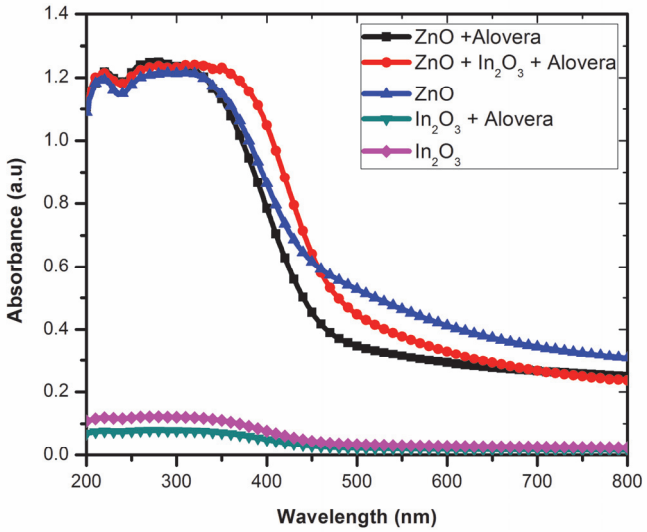

Fig. 5a: Absorption spectra of all samples except *Alovera* powder

The reflectance spectra of ZnO, In_2O_3, ZnO + *A. vera*, In_2O_3+ *A. vera*, and ZnO + In_2O_3 + *A. vera* nanocomposites are shown in Fig. 5b. In the figure, the addition of *A. vera* concentration in equal ratio to ZnO, In_2O_3, ZnO + *A. vera*, In_2O_3 + *A. vera,* and ZnO + In_2O_3 + *A. vera* resulted in diffuse reflectance increase of 89%, 60%, 45%, 40%, and 77%, respectively. These changes may be attributed to the increase in surface states of Zn and In ions and the decrease in surface defects in the other first three compounds (as confirmed by PL study). A broad reflectance peak from 530 nm to 600 nm of the compounds with *A. vera* corresponds to the dark green to reddish portion of the visible region [15].

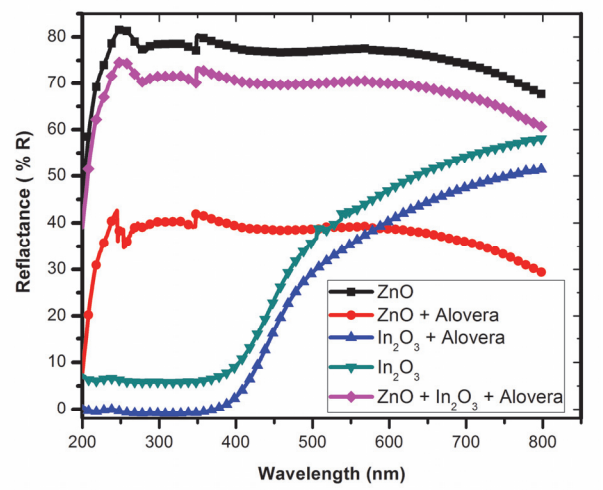

Fig. 5b: Transmission spectra of all samples except *Alovera* powder

50 nm, with a well-defined absorbance peak at around 300 nm. The direct bandgap energy (E_g) of nanocomposites is determined by fitting the absorption data to the direct transition equation:

$$\alpha h\upsilon = \mathrm{E}\,(h\upsilon - E_g)^{1/2} \quad (1)$$

where α is the optical absorption coefficient, hv is the photon energy, E_g is the direct bandgap, and E is a constant [16]. Plotting $(\alpha hv)^2$ as a function of photon energy and extrapolating the linear portion of the curve to the absorption equal, and to zero (Fig. 6) yields the following values of the direct bandgap (E_g): 3.76 eV for In_2O_3, 2.411 eV for In_2O_3 + *A. vera*, 3.544 eV for ZnO, 3.352 eV for ZnO + *A. vera*, and 3.476 eV for ZnO + In_2O_3 + *A. vera*.

UV–Vis spectroscopy was used to characterize the optical absorption properties of the nanocomposites. UV–Vis spectra were recorded in the diffuse reflectance mode (R) using $BaSO_4$ as reference. Spectra were recorded in air at room temperature, and the data was transformed through a Kubelka–Munk function relating the reflectance of the sample (Rα) to sample concentration. Mathematically, $F(R) = (1-R_\infty)^2/2R_\infty$ [17].

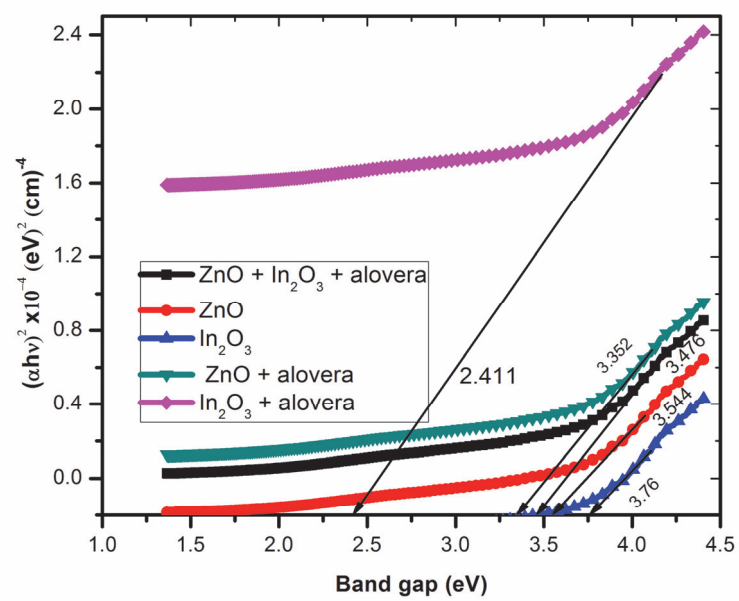

Fig. 6: Band gap values of all samples except *Alovera* powder

The PL spectra of ZnO, In_2O_3, ZnO + *A. vera*, In_2O_3 + *A. vera*, and ZnO + In_2O_3 + *A. vera* at room temperature are shown in Figs. 7 and 8. Two main bands are observed, namely, a UV emission band and a broad emission band. The UV emission band is commonly attributed to the transition in the near band-edge of ZnO + In_2O_3, particularly for nanocomposites with *A. vera* [18]. The broad emission band in the visible region (300 nm to 1200 nm) is attributed to deep-level effects in ZnO. Nanocomposites with *A. vera* are predominant and exhibit good absorbance and, consequently, good optical properties. A clear influence of the shape of particles and *A. vera* with the oxides is observed, and nanocomposite ligands are present in the PL spectra within the visible domain. Two additional emissions at 423 and 504 nm (Fig. 7) are associated with the presence of surface defects over the NPs. The first emission corresponds to the known yellow emission, whereas, for pure oxides, the second emission appears in the presence of *A. vera* and when composite ligands are present.

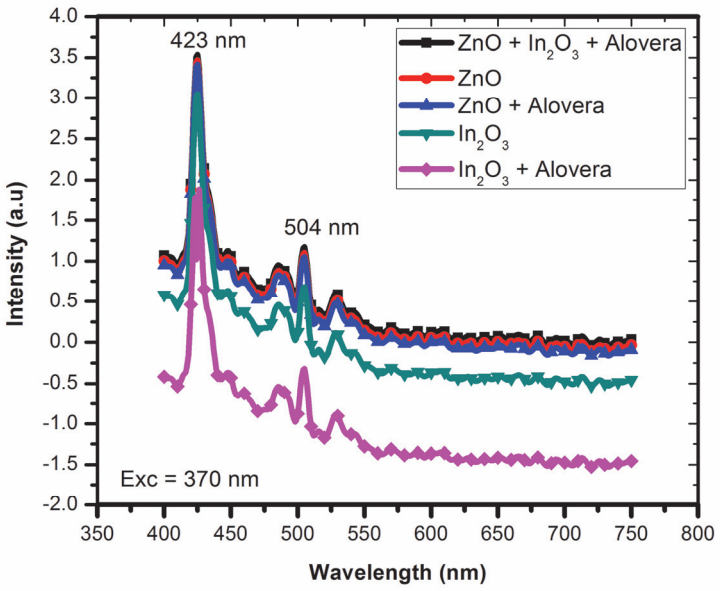

Fig. 7: Emission peak of all samples except *Alovera* powder

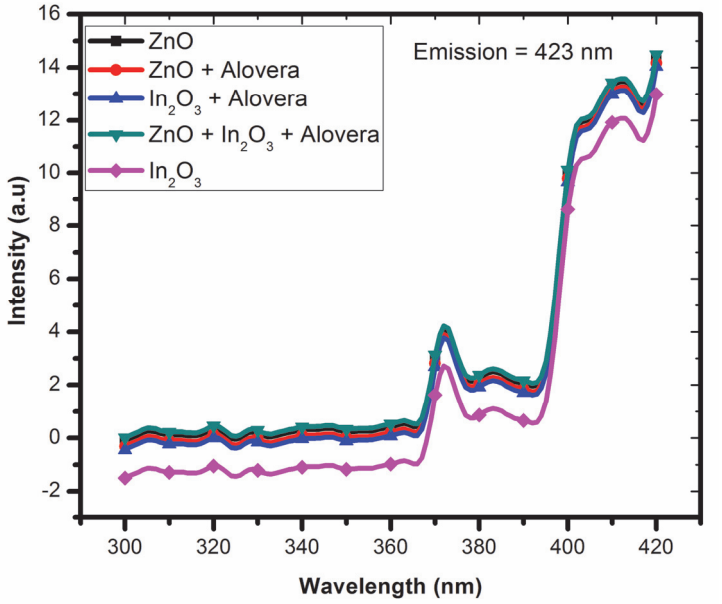

Fig. 8: Excitation peak of all sample except *Alovera* powder

3.5 Antibacterial and Antifungal Activities

NPs that are produced by plants are more stable, and the rate of synthesis is faster than in the case of microorganisms. NPs of ZnO and In_2O_3, as well as composites of ZnO + *A. vera*, In_2O_3 + *A. vera*, and ZnO + In_2O_3 + *A. vera*, vary in shape and size. The objectives of using *A. vera* extracts and semiconducting NPs in biosynthesis are interesting for investigation of the mechanisms of uptake and bioreduction of atoms and to understand the possible mechanisms and activities with five different bacteria and one fungus.

Antibacterial activity was monitored using agar–well diffusion and agar–disc diffusion method. The activity was determined by measuring the zones of inhibition around the wells or discs [19]. Antibacterial activity of *A. vera* extracts was checked against five isolates (Table 2). The percentage of Gram-positive isolates, namely, *S. aureus*, *E. coli*, *S. typhi*, and *S. pyogenes*, and the percentage of Gram-negative isolate, *P. aeruginosa*, are given. *A. vera* alone provides increasing antimicrobial and antifungal activities, which are enriched with the addition of ZnO and In_2O_3 [20].

The inhibitory effects of the pure extracts of *A. vera* powder are illustrated in Table 2. Activity-dependent and comparable results are shown in Table 2. Agar diffusion tests suggest good correlation with other antimicrobial susceptibility tests. Natural extracts of *A. vera* mixed with ZnO and In_2O_3 invariably show better performance than their original powders. No preservatives are added in the extracts and their composites to prevent biased results.

Well diffusion method was used for assessment of antibacterial activity. Antimicrobial activities of ZnO NPs against *P. aeruginosa* and *Staphylococcus* are shown in terms of inhibition zone (mm) size in Table 2.

Table 2: Antifungal activities with different microorganism of different zone of inhibition (mm)

S. No	**Bacteria**	**Zone of Inhibition (mm)**																	
		Sample A (In_2O_3 +Alovera)			Sample B (ZnO +Alovera)			Sample D (ZnO +In_2O_3 +Alovera)			Sample E (In_2O_3)			Sample F ZnO			Sample G (Alovera)		
		5 mg	10 mg	25 mg	5 mg	10 mg	25 mg	5 mg	10 mg	25 mg	5 mg	10 mg	25 mg	5 mg	10 mg	25 mg	5 mg	10 mg	25 mg
1	*Staphylococcus aureus*	7	10	19	7	12	20	8	10	22	8	12	14	14	20	24	15	17	22
2	*Escherichia coli*	-	-	-	-	-	-	7	16	20	0	16	18	-	-	-	-	-	-
3	*Salmonella*	-	-	-	14	16	20	7	9	10	-	-	-	-	-	-	-	-	-

	typhi																			
4	*Pseudomonas aeruginosa*	12	14	19	10	12	24	9	12	18	6	12	20	12	15	17	18	21	24
5	*Streptococcus pyogenes*	-	-	-	-	-	-	10	12	14	-	-	-	-	-	-	17	18	21

The antimicrobial activities of *A. vera* + ZnO NPs against *S. typhi*, *P. aeruginosa*, and *S. aureus,* as well as the antimicrobial activities of In_2O_3 NPs against *Staphylococcus*, *P. aeruginosa*, and *E. coli* are shown in terms of inhibition zone (mm). The antimicrobial activities of *A. vera* + In_2O_3 NPs against *S. aureus*, *P. aeruginosa*, and *E. coli,* as well as those of ZnO + In_2O_3 + *A. vera* NPs against *P. aeruginosa*, *S. aureus*, *S. typhi*, *E. coli*, and *S. pyogenes* are shown in terms of inhibition zone (mm) size in Figs. 9a to 9e. The antifungal activities on microorganism *A. niger* of ZnO + *A. vera* and ZnO + In_2O_3 + *A. vera* are shown in Figs. 10a and 10b, respectively. This study revealed that the tested *A. vera* plant extract exhibits potential antibacterial activity against *S. aureus* and *P. aeruginosa*. Extracts with ZnO + In_2O_3 + *A. vera* showed the highest inhibitory activity against the tested bacteria.

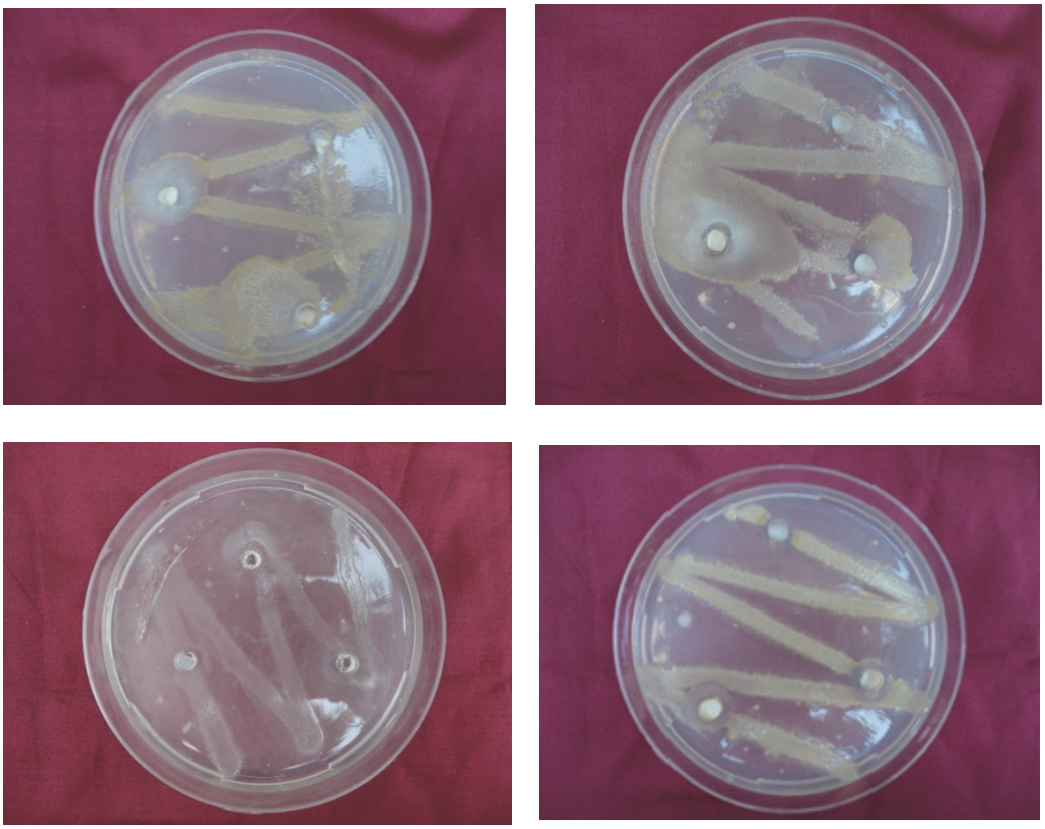

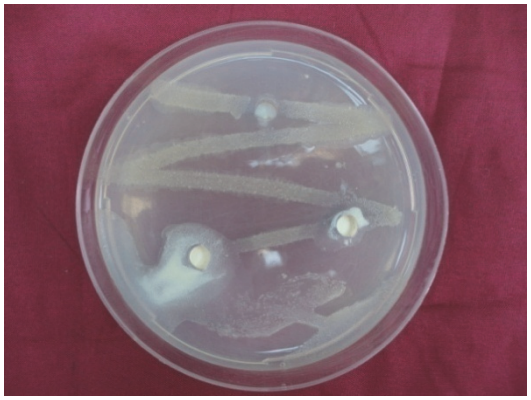

Fig. 9(a): Pseudomonas aeruginosa micro organism with (ZnO + In_2O_3 + Alovera), (b) Staphylococcus aureus micro organism with (ZnO + In_2O_3 + Alovera), (c) Salmonella typhi micro organism with (ZnO + In_2O_3 + Alovera), (d). Escherichia coli micro organism with (ZnO + In_2O_3 + Alovera), (e). Streptococcus pyogenes micro organism with (ZnO + In_2O_3 + Alovera)

The fungi tested in the ZnO + *A. vera* and ZnO + In_2O_3 + *A. vera* study presented limited susceptibility to *A. vera* gel and extracted fractions (Figs. 10a and 10b). *A. niger* growth is inhibited by the extract. This result is important because *A. niger* is resistant to both oxide NPs with *A. vera* extracts. This study has established the susceptibilities of a broad range of bacteria to fractions isolated from *A. vera* leaf extracts with oxide NPs of ZnO, In_2O_3, and ZnO + In_2O_3. Gram-negative bacilli were found to be particularly susceptible to *A. vera* extracts, ZnO, In_2O_3, and ZnO + In_2O_3 nanocomposites. Among the bacteria tested, only the Gram-positive bacteria are resistant to the *A. vera* components [21, 22].

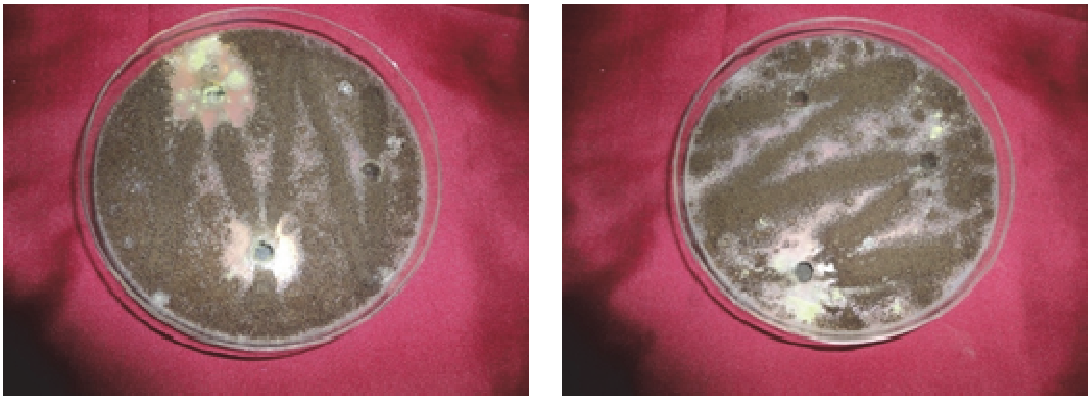

Fig. 10: (a). Antifungal activities of micro organism Aspergillus niger of (ZnO + Alovera), (b). Antifungal activities of micro organism Aspergillus niger of (ZnO + In_2O_3 + Alovera)

The antibacterial and antifungal activities of the samples with *A. vera* extracts toward five different microorganisms may be due to binding to the oxide NPs of ZnO, In_2O_3, and their nanocomposites, which resulted in novel structural, microstructural, and optical properties.

5. Conclusion

Although the synthesized ZnO and In_2O_3 nanopowders are smaller than the nanocomposites, both absorption spectra and emission show a distinct redshift with

increasing size. However, the antibacterial and antifungal activities are stronger for the nanocomposites with *A. vera*. Given that ZnO + In_2O_3 + *A. vera* are nanosized, the weakly confined quantum effects agree with those in other reports. Therefore, nanocomposites incorporated with *A. vera* offer good absorption capacity, good crystallinity, better transmission, and enhanced antibacterial and antifungal activities. ZnO, In_2O_3, ZnO + *A. vera*, In_2O_3 + *A. vera*, and ZnO + In_2O_3 + *A. vera* NPs present strong antibacterial activity against *P. aeruginosa*, and the activity is increased as the concentration of ZnO NPs is increased. The unique characteristics of NPs considerably increased the surface area of ZnO or enhanced the affinity. As a result, the ZnO NPs exhibited stronger antibacterial activity than In_2O_3.

References

[1] J. Kolnik, M. Ozvold, Phys. Stat. Solidi (a) **122** (1990) 583

[2] E. H. Rhoderick, Metal semiconductor contacts, Oxford University Press Oxford (1978)

[3]. M. Kashif, M.E.Ali, Syed M.UsmanAli, U.Hashima et al., Ceramics International **l39**, (2013) 6461–6466

[4]. A. Ayeshamariam, M.Bououdina, C.Sanjeeviraja, Materials Science in Semiconductor Processing **16** (2013) 686–695

[5] D. Zhang, C. Li, S. Han, X. Liu, T. Tang, W. Jin, C. Zhou, Appl. Phys. **A 77**, (2003), 163–166.

[6] V. H. Kasper, et al.. Anorg. Allg. Chem. **349**, (1967), 113–123.

[7]. A. Ayeshamariam, K.Tajun Meera Begam, M. Jayachandran, G. Praveen Kumar and M Bououdina, International Journal of Bioassays, ISSN: 2278-778X

[8] S. Maensiri, P. Laokul, J. Klinkaewnarong, S. Phokha, V. Promarak, S. Seraphin, J. Optoelec. Adv. Mater. 10–3 (2008), 161-165.

[9] K. Renugadevi, R.VenusAswini, Asian Journal of Pharmaceutical and clinical research, **5** (2012) 4.

[10] S .Choi, et al, British J. of Dermatol. **145** (4) (2001) 535-45.

[11] A. Surjushe, et al, Aloevera: a short review. Indian J. Dermatol. **53**(4) (2008) 163-166.

[12] M. Grieve, et al., A Modern Herbal.Jonathan Cape, London.**12** (1975) 26–9.

[13] R.K.Waihenya, M.M.Mtambo, G. Nkwengulila, U.M.Minga, et al. J. Ethnopharmacol., **79** (2002) 317-23.

[14] Z. Jindal, N. K.Verma, J. Mater. Sci. **43** (2008) 6539-6545.

[15] E. Ziegler, A. Heinrich, H. Oppermann, G. Stover, Phys. Status Solidi **A 66** (1981) 635-648.

[16] Asma Bashir, BushraSaeed, Talat .Y. Mujahid, NayarJehan et al., African J. Biotechnol., vol. **10** (19) (2011) 3835–3840.

[17] U.D. Altermatt, I.D. Brown, Ceramics Acta Crystallogr., **A 43** (1987) 121-125

[18] C. G. Granqvist, Appl. Phys. **A 57** (1993) 19-24.

[19] Lung-Chien Chen, Chih-Ming Chen, Chie-Sheng Hong J.Electrochem.Soc, **153** (2006) 931-933

[20] N.Gul , T.Y Mujahid, S. Ahmed, Pak. J. Bio. Soc. **7** (1) (2004) 2055–2060.

[21] O. Lupan, Th. Pauporte, V.V. Ursaki, I.M. Tiginyanu, Opt. Mater. **33** (2011), 914–919.

[22] O.Yamamoto, M. Hotta, J. Sawai, T. Sasamoto, H. Kojima J. Ceram. Soc. Japan.**106** (1998) 1007-11.